

Collisions of electrons with trimethylphosphine $[P(CH_3)_3]$ molecules

Alicja Domaracka, Paweł Możejko, Elżbieta Ptasińska-Denga, and Czesław Szmytkowski*
*Atomic Physics Group, Faculty of Applied Physics and Mathematics, Gdańsk University of Technology,
 ul. G. Narutowicza 11/12, 80-952 Gdańsk, Poland*
 (Received 30 July 2007; published 1 October 2007)

We report on the absolute total electron-trimethylphosphine scattering cross section (TCS) measured from 0.4 to 400 eV using a linear electron-beam attenuation method. The experimental TCS energy function exhibits very pronounced asymmetric enhancement peaked near 5.5 eV. Calculations were also carried out to obtain the integral elastic and ionization cross sections at intermediate and high energies using the independent atom and the binary-encounter-Bethe approximations, respectively. Their sum, the computed total cross section, is for intermediate energies in a reasonable agreement with the present experimental TCS data. Furthermore, the measured TCS for $P(CH_3)_3$ is compared with the TCSs for some other phosphines [PH_3 , PF_3] and other methides [$B(CD_3)_3$, $N(CH_3)_3$]. Analysis clearly shows that exterior atoms of a molecule influence the scattering process more significantly than the central atom.

DOI: [10.1103/PhysRevA.76.042701](https://doi.org/10.1103/PhysRevA.76.042701)

PACS number(s): 34.80.Bm, 34.80.Gs

I. INTRODUCTION

Knowledge of elementary physicochemical events, among them those involving electrons, occurring in media of technological interest for fabrication of large-scale integrated electronic circuits, is of great importance for understanding, modeling, and controlling the gas phase reactions in facilities used for materials processing; see, e.g., Ref. [1]. Trimethylphosphine (TMP) $[P(CH_3)_3]$ is an organic compound which has recently been considered to be a promising P-doping source, replacing the less friendly PH_3 gas, in preparation of nanometer-scale structures in silicon [2,3] and/or diamond films [4,5] manufactured for electronic devices.

There are, to date, only a few experimental studies of electron interactions with trimethylphosphine. Early works with TMP, involving electrons as projectile, focused on the high-energy electron diffraction [6] and the electron impact ionization [7,8]. In later investigations of e -TMP processes, low-energy electron transmission spectroscopy that reported resonant effects [9,10] and electron momentum spectroscopy [11] were used. In the literature, one can also find recent experiments on the adsorption and decomposition of TMP on the Pt(111) [12] and Si(111) surfaces [2] carried out with high-resolution electron energy-loss spectroscopy. However, none of the aforementioned works presents the electron scattering intensities in an absolute scale. To our knowledge, theoretical works on the electron-assisted processes with TMP have not yet been reported in the literature.

In this paper, we present the absolute electron-scattering grand total cross section (TCS) for trimethylphosphine measured from 0.4 to 400 eV by means of an electron transmission method. As the TCS is obtained without any normalization procedure, it is especially valuable as one of the quantitative tests for theoretical computations, and is also useful for normalization of electron-scattering quantities taken in relative units. In principle, the grand TCS, which

comprises summary information on all scattering processes, provides little detail of the individual scattering channels. However, the structures visible in the TCS energy function may give some clue of their possible origin and directly point out the regions of energy worth more detailed investigations. In addition to the experiment, the integral elastic and ionization cross sections have been calculated at intermediate and high energies using simple theoretical models: the independent atom (IA) model and binary-encounter-Bethe (BEB) approach, respectively. The sum of elastic and ionization cross section, which stands for computed total cross section, is compared with experimental findings. The similarities and differences in electron-scattering TCS energy dependences for series of phosphorus-containing [PH_3 , PF_3 , and $P(CH_3)_3$] and permethylated [$B(CD_3)_3$, $N(CH_3)_3$, and $P(CH_3)_3$] molecules are indicated; the role of the atom location in molecule is also discussed.

II. EXPERIMENT

For present measurements of the absolute e - $P(CH_3)_3$ scattering total cross section (TCS) a linear electron-transmission method has been used. In the experimental setup applied, the quasimonoenergetic electron beam [$\Delta E \approx 90$ meV, full width at half maximum (FWHM)] is led through the reaction cell filled with vapor of the compound under study. Electrons which pass through the interaction region and emerge from the cell exit aperture cross a retarding-field lens system, and are collected with a Faraday cup. The transparency of the target vapor to the electron beam of a given energy E depends inversely on the electron-scattering cross section at this energy. The electron-scattering total cross section [$Q(E)$] is—in the reported experiment—derived from the Bouguer-de Beer-Lambert (BBL) attenuation law

$$I(p, E) = I(p=0, E) \exp\left(-\frac{pL}{k\sqrt{T_m T_c}} Q(E)\right),$$

in which $I(p, E)$ and $I(p=0, E)$ are the intensities of the transmitted electron currents in the presence and absence of

*cysz@mif.pg.gda.pl

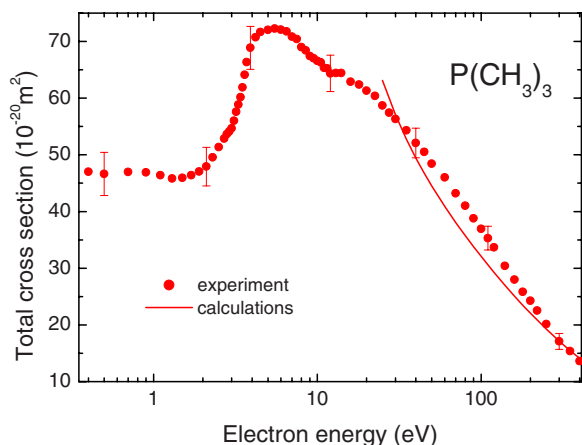


FIG. 1. (Color online) Total cross sections for e - $P(\text{CH}_3)_3$ scattering. Full circles indicate the present TCS measurements (error bars represent overall experimental uncertainties). Computed cross section (full line) is the sum of the elastic and ionization contributions (ECS+ICS) calculated in the IAM approach with the SP potential and in the BEB approximation, respectively.

the target molecules in the scattering cell, respectively; p is the pressure of the investigated target in the cell of length L ($=30.5$ mm); T_c is the temperature of the scattering cell (310–320 K), while T_m ($=322$ K) is the temperature of the capacitance mks manometer sensor, and k stands for the Boltzmann constant; note that the thermal transpiration effect [13] is accounted for in the BBL formula. The electron energy scale is established, within an accuracy of about 0.1 eV, against the oscillatory structure appearing around 2.3 eV in the transmitted current when molecular nitrogen is admixed to the compound under study. The absence of magnetic and electric fields in the scattering and detector volume enables us to give more accurate estimate of the path on which scattering takes place, and of the solid angle (0.4 msr) of the detector system. The sample of trimethylphosphine (97% pure from Aldrich) was used as supplied without further purification other than vacuum distillation. The whole target handling system has been kept at elevated temperature of about 310 K. The electron spectrometer used in the present experiment was already employed in our previous systematic TCS studies, and more details on the apparatus and measuring procedure can be found elsewhere (e.g., Refs. [14,15]).

The measurements were carried out for a given electron impact energy in a series of runs using a range of target pressures and various sets of electron-beam controlling parameters. The final TCS values are the weighted means of the average from different measurement series for the same impact energy. The overall experimental errors, as marked in Fig. 1, are the summed uncertainties of random and systematic nature. The statistical uncertainty of the resulting TCS (one standard deviation of the weighted mean value) is well below 1% over the whole electron energy range applied. Among many effects which may systematically distort the individual quantities measured in the present experiment, and therefore may contribute to the overall systematic TCS uncertainty, two are because of the difficulties to meet exactly the conditions at which the BBL formula is fully satis-

fied. The first one is associated with the imperfect discrimination, by the detector system, of electrons scattered into small forward angles—that systematically lowers the derived TCS values. We estimate that for the geometry of our electron collector system, the lessening of the measured TCS should not exceed 2–3 % at the lowest and highest applied energies. The second factor affecting the measured TCS is related to the unavoidable effusion of target molecules throughout the apertures of the reaction cell, through which electrons enter and leave the target volume. This end effect does not allow an accurate determination of the numerator pL in the BBL formula. The uncertainty related to that factor was estimated to be lower than 2.5% (see Ref. [16]). To reduce the influence of the target molecules (effusing from the reaction cell apertures) on the electron optics elements and, consequently, on the intensity of the primary electron beam, (i) the whole electron optics was immersed in target vapor for one day before the measurements, whereas (ii) in the course of the experiment, the vapor was allowed alternately into the reaction cell and the electron optics volume (through a by-pass valve), so the partial target pressure in the electron optics region (about 0.2 mPa) was constant, irrespective of whether the target was present or not in the cell. Notable contribution to the systematic TCS inaccuracy may arise also from the impurity of the sample. A sum of all individual potential uncertainties amounts to about 7–9% below 2 eV, decreasing gradually to 6% between 5–150 eV, and increasing again up to 8% at the highest energies applied.

III. THEORETICAL METHODS

To estimate the total cross section for the e - $P(\text{CH}_3)_3$ scattering at incident energies extending over those used in the reported experiment we have performed simple but quite credible numerical calculations. As in our previous works (e.g., Refs. [17,18]), the computed total cross section is estimated as a sum of the elastic (ECS) and ionization (ICS) cross sections. This approach is rather rough because in addition to elastic scattering only the ionization is taken into account while other inelastic channels are neglected. On the other hand, we have found that total cross sections (elastic + ionization) estimated this way satisfactorily reproduce the intermediate energy experimental data for a variety of molecular polyatomic targets ([17,18], and references therein).

Ionization cross section has been calculated using the binary-encounter-Bethe (BEB) model [19,20]. Within that model the electron-induced ionization cross section for molecule can be obtained as

$$\sigma^{\text{ion}}(E) = \sum_{i=1}^{n_{\text{MO}}} \sigma_i^{\text{BEB}}, \quad (1)$$

where n_{MO} is the number of the given molecular orbital. The ionization cross section per molecular orbital is given by

$$\sigma^{\text{BEB}} = \frac{S}{\epsilon + u + 1} \left[\frac{\ln \epsilon}{2} \left(1 - \frac{1}{\epsilon^2} \right) + 1 - \frac{1}{\epsilon} - \frac{\ln \epsilon}{\epsilon + 1} \right], \quad (2)$$

TABLE I. Comparison of experimental and theoretical ionization potentials for selected molecular orbitals of the $\text{P}(\text{CH}_3)_3$ molecule; in eV.

Orbital	Expt. [26]	[27]	[28]	Present
$5a_1$				27.85
$3e$	19.6	19.53		25.65
$6a_1$		15.75		17.77
$7a_1$		13.13	15.88	14.98
$4e$	15.8	13.07	15.89	14.65
$5e$	12.7	12.11	14.63	13.96
$1a_2$		12.01	13.87	13.63
$6e$	11.3	10.67	12.04	11.14
$8a_1$	8.58	8.41	8.49	8.159

where $u = U/B$, $\epsilon = E/B$, $S = 4\pi a_0^2 N R^2 / B^2$ ($a_0 = 0.5292 \text{ \AA}$, $R = 13.61 \text{ eV}$), and E is the energy of the impinging electron. The electron binding energy B average kinetic energy of electron on the given orbital U and orbital occupation number N have been calculated for the ground states of the geometrically optimized (within C_{3v} symmetry) molecule with the Hartree-Fock method using the GAUSSIAN code [21], and the Gaussian 6-311G+ basis set. Because energies of the highest occupied molecular orbitals (HOMOs) obtained this way usually differ from experimental ones, we also performed the outer valence Green function calculations of correlated electron affinities and ionization potentials [22–25] using GAUSSIAN [21]. The resulting values of the ionization potentials for selected orbitals are listed and compared with available experimental [26] and theoretical [27,28] data in Table I.

The elastic electron interaction with $\text{P}(\text{CH}_3)_3$ molecules has been studied using the additivity rule (e.g., Refs. [29,30]) in which the molecular elastic cross section is given by

$$\sigma^{\text{mol}}(E) = \sum_{i=1}^{N_A} \sigma_i^A(E), \quad (3)$$

where E is the energy of the incident electron. The elastic cross section for the i th atom of the target molecule $\sigma_i^A(E)$ has been derived according to

$$\sigma^A = \frac{4\pi}{k^2} \left(\sum_{l=0}^{l_{\text{max}}} (2l+1) \sin^2 \delta_l + \sum_{l=l_{\text{max}}}^{\infty} (2l+1) \sin^2 \delta_l^{(B)} \right). \quad (4)$$

To obtain phase shifts δ_l , partial wave analysis has been employed and the radial Schrödinger equation

$$\left[\frac{d^2}{dr^2} - \frac{l(l+1)}{r^2} - 2[V_{\text{stat}}(r) + V_{\text{polar}}(r)] + k^2 \right] u_l(r) = 0 \quad (5)$$

has been solved numerically under the boundary conditions

$$u_l(0) = 0, \quad u_l(r) \sim A_l \hat{j}_l(kr) - B_l \hat{n}_l(kr), \quad (6)$$

where $\hat{j}_l(kr)$ and $\hat{n}_l(kr)$ are the Riccati-Bessel and Riccati-Neumann functions, respectively. In the present calculations the electron-atom interaction is represented by static $V_{\text{stat}}(r)$ [31] and polarization $V_{\text{polar}}(r)$ [32] potentials, which are given by the following expressions:

$$V_{\text{stat}}(r) = -\frac{Z}{r} \sum_{m=1}^3 \gamma_m \exp(-\beta_m r),$$

where Z is the nuclear charge of the atom, γ_m and β_m are parameters derived by numerical fitting to the numerical Dirac-Hartree-Fock-Slater screening function [31]

$$V_{\text{polar}}(r) = \begin{cases} \nu(r), & r \leq r_c, \\ -\alpha/2r^4, & r > r_c, \end{cases}$$

where $\nu(r)$ is the free-electron-gas correlation energy [33], α is the static electric dipole polarizability of the atom, and r_c is the first crossing point of the curves of $\nu(r)$ and $-\alpha/2r^4$ [34]. In the present calculations, the exact phase shifts have been calculated for l up to $l_{\text{max}} = 50$, while those remaining $\delta_l^{(B)}$ have been included through the Born approximation. Final values of integral elastic and ionization cross sections calculated up to 3 keV for $\text{P}(\text{CH}_3)_3$ are listed in Table II.

IV. RESULTS AND DISCUSSION

In this section we present our absolute total electron-scattering cross-section (TCS) for trimethylphosphine $\text{P}(\text{CH}_3)_3$ measured in the linear electron-transmission experiment over energy range from 0.4 to 400 eV. We compare these experimental TCS data with our intermediate-energy theoretical results, in the overlapping energy range. Afterwards, we analyze the variation of the TCS across series of phosphorus-containing compounds [PH_3 , PF_3 , $\text{P}(\text{CH}_3)_3$] and of permethylated [$\text{B}(\text{CD}_3)_3$, $\text{N}(\text{CH}_3)_3$, $\text{P}(\text{CH}_3)_3$] molecules.

A. Trimethylphosphine $\text{P}(\text{CH}_3)_3$

Figure 1 shows the absolute total electron-scattering cross section for $\text{P}(\text{CH}_3)_3$ molecule as a function of energy measured from 0.4 to 400 eV. Experimental TCS values versus electron impact energy are also listed in Table III. The measurements are confronted, in deficiency of other TCS data, with the intermediate-energy “total” cross section calculated here, composed of the integral elastic (ECS) and total ionization (ICS) cross sections.

There are two characteristics of the measured TCS for e - $\text{P}(\text{CH}_3)_3$ scattering: (i) the very strong and highly asymmetric enhancement peaking around 5.5 eV and (ii) the relatively large magnitude of the TCS over the whole energy range investigated. At the lowest energies applied, between 0.4 and 2 eV, the TCS is a slowly varying function of energy, within $45\text{--}46 \times 10^{-20} \text{ m}^2$. Such behavior of the TCS low-energy dependence is somewhat intriguing as $\text{P}(\text{CH}_3)_3$ is a moderately polar molecule (see Table IV) so one might rather expect an increase of cross section toward the lowest energies. Above 2 eV the TCS rises steeply and in the vicinity of 5.5 eV it reaches its maximum value of about 72

TABLE II. Ionization (ICS) and integral elastic (ECS) cross sections calculated for electron impact on P(CH₃)₃ molecules; in 10⁻²⁰ m².

<i>E</i> (eV)	ICS	ECS	<i>E</i> (eV)	ICS	ECS	<i>E</i> (eV)	ICS	ECS
8.159	0.00		50	12.6	31.9	300	7.91	9.22
9	0.156		60	13.1	27.8	350	7.21	8.27
10	0.351		70	13.2	24.9	400	6.62	7.50
11	0.539		80	13.1	22.7	450	6.13	6.88
12	0.878		90	12.9	20.9	500	5.71	6.36
14	1.61		100	12.7	19.5	600	5.03	5.54
16	2.84		110	12.4	18.2	700	4.50	4.93
18	4.11		120	12.1	17.2	800	4.08	4.44
20	5.30	67.1	140	11.5	15.5	900	3.73	4.05
25	7.66	55.5	160	10.9	14.2	1000	3.45	3.73
30	9.41	47.6	180	10.3	13.1	2000	1.99	2.22
35	10.7	42.1	200	9.85	12.2	2500	1.66	1.96
45	12.2	34.5	250	8.78	10.5	3000	1.42	1.85

× 10⁻²⁰ m². The maximum is followed by a broad shoulder extended from 14 to about 25 eV. Beyond 30 eV the TCS becomes monotonously descending function of impact energy. Starting from 60 eV, the energy dependence of the experimental TCS for *e*-P(CH₃)₃ scattering behaves as $Q(E) \sim E^{-0.6}$. At 400 eV TCS falls to about 14×10^{-20} m².

A closer inspection of the low-energy side of the TCS curve reveals three weak features: a hump centered near 0.8 eV, a shallow minimum located at 1.3 eV, and a shoulder on the steep slope of the TCS enhancement near 3 eV. Though these features are only just visible they were repetitious in all series of the experiment. The poorly resolved narrow 3 eV

TABLE III. Absolute electron-scattering total cross sections for P(CH₃)₃ molecules in 10⁻²⁰ m².

<i>E</i> (eV)	TCS	<i>E</i> (eV)	TCS	<i>E</i> (eV)	TCS
0.4	47.0	4.2	70.4	27.5	57.4
0.5	46.6	4.5	71.6	30	56.3
0.7	47.0	5.0	72.0	35	54.3
0.9	46.9	5.5	72.3	40	52.1
1.1	46.4	6.0	72.1	45	50.5
1.3	45.8	6.5	71.8	50	48.4
1.5	46.0	7.0	70.9	60	46.0
1.7	46.4	7.5	70.4	70	43.2
1.9	47.1	8.0	69.0	80	41.0
2.1	47.9	8.5	68.4	90	38.8
2.3	49.6	9.0	67.4	100	36.9
2.5	51.4	9.5	67.1	110	35.3
2.7	52.8	10.0	66.6	120	33.7
2.8	53.6	10.5	66.3	140	30.4
2.9	54.1	11.0	65.7	160	28.0
3.0	54.7	11.5	65.2	180	25.8
3.1	56.0	12	64.4	200	24.3
3.2	57.6	13	64.2	220	22.5
3.3	58.9	14	64.1	250	20.2
3.4	60.2	16	63.2	300	17.1
3.5	61.8	18	62.4	350	15.4
3.6	64.1	20	61.3	400	13.6
3.7	66.4	22.5	60.4		
3.9	68.9	25	58.7		

TABLE IV. Molecular electric dipole moments μ , electric dipole polarizabilities α , ionization potentials (IP), and the gas-kinetic cross sections σ_{gk} for some phosphorus-containing and permethylated molecules; the data printed in italics are estimated in this work (see text), others are from Refs. [11,42–45].

Molecule	μ (Debye)	α (10^{-30} m ³)	IP (eV)	σ_{gk} (10^{-20} m ²)
PH ₃	0.58	4.84	9.87	9.32
PF ₃	1.1	4.43	11.6	10.9
P(CH ₃) ₃	1.2	8–10	8.1–9.2	<i>16–18</i>
N(CH ₃) ₃	0.61	8.15	7.82	15.5
B(CD ₃) ₃	0	8.0–8.3	10.7	<i>15–16</i>

shoulder corresponds to the 3.1 eV resonant feature clearly visible in the derivative electron transmission (DET) spectra obtained by the Maryland group [9,10]; the DET spectroscopy is especially suitable for the detection of weak resonant structures in the cross section energy function. According to DET experiments [9,10], around 3.1 eV a temporary parent anion arises when the projectile electron is trapped into the low-lying empty molecular orbital, with predominant $\sigma_{\text{p-C}}^*$ character. The negative-ion shape resonance promptly decays to the parent molecule in a ground or an excited state with the emission of the extra electron, or decomposes into negative fragment ion and neutral. Lack of more detailed studies does not allow us to specify which decay channel contributes more to the 3 eV structure. Anyhow, one can assume that overall resonant contribution to the TCS near 3 eV is rather low, of the range 1×10^{-20} m², too small to be clearly resolved on the steep slope of TCS of such a large (54×10^{-20} m²) value. In the range of the broad TCS enhancement one would also expect the formation of further resonant states. The basis for such a statement has been already provided by the DET spectra of Giordan *et al.* [10] in which the broad shape resonance located around 5.5 eV is discernible. Unfortunately, the scarcity of studies for particular *e*-P(CH₃)₃ scattering processes (especially elastic and vibrational) in this energy range allows only speculation on the origin of the broad TCS structure. The inspection of the electron-scattering data (in Ref. [35]) available for other polyatomic molecules indicates that the low-energy TCS enhancement is dominated by the elastic channel with some minor vibrational contributions. The broadening of the *e*-P(CH₃)₃ enhancement around 5.5 eV suggests that the peak probably originates from the overlap of shallow broad structures associated with the formation of two or more resonant states in the range of the peak. The absence of any bands in the peak region may also arise from the superposition of structures, associated with the resonant excitation of variety of vibrational modes of the P–C bond and CH₃ group, peaking at different energies [36]. As P(CH₃)₃ molecule comprises three CH₃ radicals which may easily rotate around the P–C bond, these resonant structures become blurred and, in consequence, are not distinguishable on the elastic TCS background. The possibility of such an effect follows from the elastic calculations of Varella *et al.* [37] for

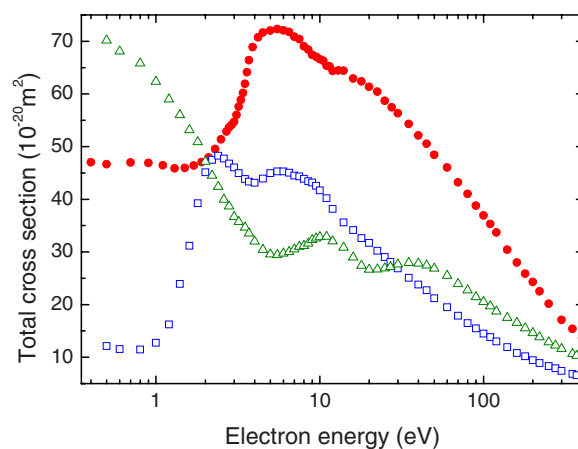


FIG. 2. (Color online) Comparison of the experimental electron-scattering TCS for some phosphorus containing molecules: P(CH₃)₃ (full circles), present; PF₃ (open triangles), from Ref. [39]; PH₃ (open squares), from Ref. [38].

two conformers of trimethylarsine, a homolog of trimethylphosphine. The shoulder spanned between 14 and 25 eV may result from superposition of numerous weak resonant effects as well as direct processes allowed in this energy range.

The calculated intermediate-energy “total” cross section (elastic+ionization) appears to be in reasonable agreement with experimental TCS according to the shape but it becomes distinctly higher than measurements below 30 eV, 9–14 % lower around 100 eV, and merging the measurements above 250 eV, as presented in Fig. 1. The disagreement below 30 eV is presumably due to the limitations of the independent atom model applied for elastic calculations. The difference around 100 eV is associated mainly with underestimation of inelastic contribution in this energy range, as only the ionization is taken into account. Based on good agreement between calculations and the experiment between 250 and 400 eV, one can conclude that our calculations also reasonably represent the TCS for higher energies.

B. Comparison of TCSs for phosphorus-containing compounds PH₃, PF₃, and P(CH₃)₃

Figure 2 compares the TCS for electron scattering from three phosphorus-containing molecules: PH₃ (from Ref. [38]), its perfluorinated PF₃ (from Ref. [39]), and permethylated P(CH₃)₃ (present) analogs. All three molecules have triangle pyramid geometry with the phosphorus atom located on the top and different exterior atoms: hydrogen, fluorine, and the methyl groups. The substitution of the outermost atoms in phosphines changes the distribution of electric charge in the resulting molecules and the response of the molecular electron cloud to the impinging electron. That means that the atom substitution changes the long-range part of the potential which the projectile electron suffers approaching the target molecule what should be reflected in the relevant electron-scattering cross section.

It is clearly illustrated by Fig. 2 in which phosphines substituted with different external atoms have TCS energy func-

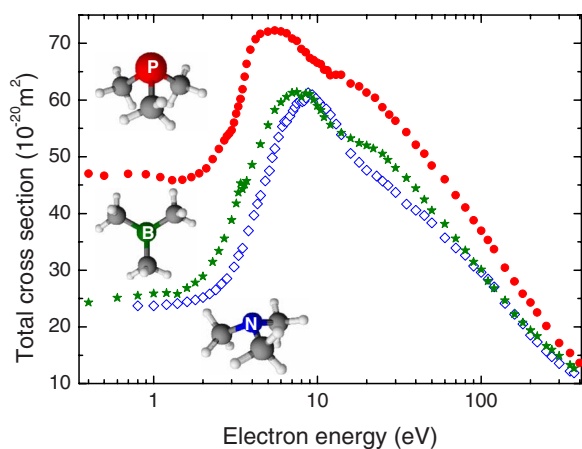


FIG. 3. (Color online) Comparison of the present measured total e - $\text{P}(\text{CH}_3)_3$ cross section (full circles) with cross sections measured for some permethylated compounds: $\text{N}(\text{CH}_3)_3$ (open diamonds), from Ref. [18]; $\text{B}(\text{CD}_3)_3$ (full stars), from Ref. [38]. Schematic geometry of molecules is included.

tions essentially different in the shape and magnitude. The substitution effect is the most pronounced at low incident energies. According to the general shape, TCS energy dependences for PH_3 and $\text{P}(\text{CH}_3)_3$ look somewhat similar, although the curve for the later molecule is distinctly shifted toward higher energies, e.g., the first maximum from 2.3 eV for PH_3 to about 5.5 eV for $\text{P}(\text{CH}_3)_3$. Replacement of hydrogen atoms in PH_3 by methyl groups distinctly changes the size of the molecule which results in an increase of magnitude of the respective TCSs of about 2 times. Starting from 20 eV, TCSs for PH_3 and $\text{P}(\text{CH}_3)_3$ become monotonously decreasing functions of energy, similar to other hydrogen-containing targets [40]. For the PF_3 molecule a characteristic increase of TCS around 40 eV (perfluorination effect) is clearly seen in Fig. 2.

C. Comparison of TCSs for permethylated compounds $\text{P}(\text{CH}_3)_3$, $\text{N}(\text{CH}_3)_3$, and $\text{B}(\text{CD}_3)_3$

Figure 3 compares the TCSs for electron scattering by three permethylated molecules $\text{B}(\text{CD}_3)_3$ [17], $\text{N}(\text{CH}_3)_3$ [18], and $\text{P}(\text{CH}_3)_3$ (present). The central atom (B, N, and P) of each molecule is enveloped with three methyl groups. The molecules differ in geometry (see Fig. 3): $\text{B}(\text{CD}_3)_3$ is a planar of D_{3h} symmetry with the B atom in the center, while $\text{N}(\text{CH}_3)_3$ and $\text{P}(\text{CH}_3)_3$ have pyramidal geometry (C_{3v}) with the “central” atom on the top.

Regarding the shape, the compared TCS curves generally resemble each other; they all have distinct enhancement with the maximum located below 10 eV which for each considered methide is slightly shifted with respect to others. On the low-energy side, below 2 eV, these TCSs are nearly constant, both for nonpolar [$\text{B}(\text{CD}_3)_3$] and polar [$\text{N}(\text{CH}_3)_3$, $\text{P}(\text{CH}_3)_3$] molecules. On the left-hand slope of the TCS enhancement very weak feature is discernible in each curve which may be attributed to resonant capture by molecule of the impinging electron into antibonding orbital located mainly on the

carbon—central-atom bond. The main maxima are distinctly broadened, probably due to overlapping of structures associated with two or more resonant states formed within region of the maximum and obscured because of conformation of methyl groups [36,37]. For $\text{B}(\text{CD}_3)_3$ and $\text{N}(\text{CH}_3)_3$, however, some weak features on the maximum ridge are discernible while they are smeared up in the $\text{P}(\text{CH}_3)_3$ curve. In the vicinity of 20 eV, in each curve more or less distinct shoulder is visible which may also be resonant in the origin. Intermediate-energy TCS behavior for compared methides can be expressed by the same regression relationship $Q(E) \sim E^{-a}$, with $a \approx 0.6$. Such a value of the exponent in the energy dependence is characteristic for targets with the envelope from hydrogen atoms; for perfluorinated molecules the exponent $a \leq 0.5$.

The variation in the TCS magnitude, when going from one considered target to another, can be presumably explained in terms of the molecular size of targets. The TCSs for $\text{B}(\text{CD}_3)_3$ and $\text{N}(\text{CH}_3)_3$ are nearly equal to each other, within experimental uncertainties, over the whole energy range investigated. Similar behavior of TCSs, especially above 10 eV, was noticed earlier for BF_3 and NF_3 molecules [39,41] which have a geometry similar to their respective permethylated counterparts. Moreover, BF_3 and NF_3 also have very close gas-kinetic cross sections (as deduced from the van der Waals b parameter [42]). Considering the aforementioned similarities we have concluded that $\text{B}(\text{CD}_3)_3$ has the gas-kinetic cross section nearly the same as $\text{N}(\text{CH}_3)_3$ (see Table IV). The distinct increase of the TCS for $\text{P}(\text{CH}_3)_3$ in comparison to those for $\text{B}(\text{CD}_3)_3$ and $\text{N}(\text{CH}_3)_3$ can be accounted through much larger molecular size of $\text{P}(\text{CH}_3)_3$ molecule.

V. SUMMARY

We have measured the absolute total electron-scattering cross section for the $\text{P}(\text{CH}_3)_3$ molecule from 0.4 to 400 eV employing a linear transmission technique. The experimental TCS energy dependence for $\text{P}(\text{CH}_3)_3$ shows very distinct, highly asymmetric, enhancement peaked near 5.5 eV. Two TCS features, the shoulder near 3 eV and maximum around 5.5 eV may be ascribed to formation of short-lived negative-ion resonant states. We have also carried out calculations of the integral elastic and total ionization cross sections from intermediate up to 3 keV incident energies. Agreement between the present computed total cross section (integral elastic+ionization) and experimental intermediate-energy TCS is reasonable. We have also compared the TCS energy functions for phosphorus-containing PX_3 ($X=\text{H}, \text{F}, \text{CH}_3$) and for permethylated [$\text{P}(\text{CH}_3)_3$, $\text{N}(\text{CH}_3)_3$, and $\text{B}(\text{CD}_3)_3$] molecules to examine how the substitution of the central atom and/or outer atoms influences the TCS energy function. Our data show that the substitution of the exterior atoms changes the low-energy TCS essentially, both in the shape and magnitude. At intermediate energies the only difference is the change of the TCS magnitude following the molecular size. Substitution effect of the central atom in methides is less visible because of the screening effect of the exterior methyl

groups. To complement these observations, we noticed on basis of our systematic TCS experiments that at intermediate energies where direct scattering processes dominate there is evident a straightforward relation between the size of the target molecule and the magnitude of the respective intermediate TCS.

ACKNOWLEDGMENTS

This work is part of the MNSzW program 2007–2008 and is supported by the Polish Ministry of Science and Higher Education (Project No. N202 110 32/2862). Numerical calculations have been performed at the Academic Computer Center (TASK) in Gdańsk.

- [1] L. G. Christophorou and J. K. Olthoff, *Fundamental Electron Interactions with Plasma Processing Gases* (Kluwer Academic, New York, 2004), and references therein.
- [2] Y. Fukuda, M. Shimomura, G. Kaneda, N. Sanada, V. G. Zavodinsky, I. A. Kuyanov, and E. N. Chukurov, *Surf. Sci.* **442**, 507 (1999).
- [3] G. M. Oleszek, *J. Electrochem. Soc.* **148**, G215 (2001).
- [4] H. Wada, T. Teraji, and T. Ito, *Appl. Surf. Sci.* **244**, 305 (2005).
- [5] H. Kato, W. Futako, S. Yamasaki, and H. Okushi, *Diamond Relat. Mater.* **14**, 340 (2005).
- [6] H. D. Springall and L. O. Brockway, *J. Am. Chem. Soc.* **60**, 996 (1938); L. S. Bartell and L. O. Brockway, *J. Chem. Phys.* **32**, 512 (1960).
- [7] M. Halmann, *J. Chem. Soc.* **1962**, 3270; J. Fischler and M. Halmann, *ibid.* **1964**, 31.
- [8] Y. Wada and R. W. Kiser, *J. Phys. Chem.* **68**, 2290 (1964).
- [9] J. A. Tossell, J. H. Moore, and J. C. Giordan, *Inorg. Chem.* **24**, 1100 (1985).
- [10] J. C. Giordan, J. H. Moore, J. A. Tossell, and W. Kaim, *J. Am. Chem. Soc.* **107**, 5600 (1985); J. C. Giordan, J. H. Moore, and J. A. Tossell, *Acc. Chem. Res.* **19**, 281 (1986).
- [11] J. Rolke and C. E. Brion, *Chem. Phys.* **207**, 173 (1996).
- [12] G. E. Mitchell, M. A. Henderson, and J. M. White, *J. Phys. Chem.* **91**, 3808 (1987).
- [13] M. Knudsen, *Ann. Phys.* **31**, 205 (1910).
- [14] Cz. Szymkowski, P. Możejko, and G. Kasperski, *J. Phys. B* **31**, 3917 (1998).
- [15] Cz. Szymkowski and P. Możejko, *Vacuum* **63**, 549 (2001).
- [16] R. N. Nelson and S. O. Colgate, *Phys. Rev. A* **8**, 3045 (1973).
- [17] A. Domaracka, P. Możejko, E. Ptasińska-Denga, and Cz. Szymkowski, *J. Phys. B* **39**, 4289 (2006).
- [18] Cz. Szymkowski, A. Domaracka, P. Możejko, and E. Ptasińska-Denga, *Phys. Rev. A* **75**, 052721 (2007).
- [19] Y.-K. Kim and M. E. Rudd, *Phys. Rev. A* **50**, 3954 (1994).
- [20] W. Hwang, Y.-K. Kim, and M. E. Rudd, *J. Chem. Phys.* **104**, 2956 (1996).
- [21] M. J. Frisch, G. W. Trucks, H. B. Schlegel, G. E. Scuseria, M. A. Robb, J. R. Cheeseman, J. A. Montgomery, Jr., T. Vreven, K. N. Kudin, J. C. Burant, J. M. Millam, S. S. Iyengar, J. Tomasi, V. Barone, B. Mennucci, M. Cossi, G. Scalmani, N. Rega, G. A. Petersson, H. Nakatsuji, M. Hada, M. Ehara, K. Toyota, R. Fukuda, J. Hasegawa, M. Ishida, T. Nakajima, Y. Honda, O. Kitao, H. Nakai, M. Klene, X. Li, J. E. Knox, H. P. Hratchian, J. B. Cross, C. Adamo, J. Jaramillo, R. Gomperts, R. E. Stratmann, O. Yazyev, A. J. Austin, R. Cammi, C. Pomelli, J. W. Ochterski, P. Y. Ayala, K. Morokuma, G. A. Voth, P. Salvador, J. J. Dannenberg, V. G. Zakrzewski, S. Dapprich, A. D. Daniels, M. C. Strain, O. Farkas, D. K. Malick, A. D. Rabuck, K. Raghavachari, J. B. Foresman, J. V. Ortiz, Q. Cui, A. G. Baboul, S. Clifford, J. Cioslowski, B. B. Stefanov, G. Liu, A. Liashenko, P. Piskorz, I. Komaromi, R. L. Martin, D. J. Fox, T. Keith, M. A. Al-Laham, C. Y. Peng, A. Nanayakkara, M. Challacombe, P. M. W. Gill, B. Johnson, W. Chen, M. W. Wong, C. Gonzalez, and J. A. Pople, *GAUSSIAN 03*, Revision B.03 (Gaussian, Pittsburgh, 2003).
- [22] L. S. Cederbaum, *J. Phys. B* **8**, 290 (1975).
- [23] W. von Niessen, J. Schirmer, and L. S. Cederbaum, *Comput. Phys. Rep.* **1**, 57 (1984).
- [24] J. V. Ortiz, *J. Chem. Phys.* **89**, 6348 (1988).
- [25] V. G. Zakrzewski and W. von Niessen, *J. Comput. Chem.* **14**, 13 (1993).
- [26] J. P. Maier and D. W. Turner, *J. Chem. Soc., Faraday Trans.* **2**, 711 (1972).
- [27] S.-X. Xiao, W. C. Trogler, D. E. Ellis, and Z. Berkovitch-Yellin, *J. Am. Chem. Soc.* **105**, 7033 (1983).
- [28] I. H. Hillier and V. R. Saunders, *Trans. Faraday Soc.* **66**, 2401 (1970).
- [29] D. Raj, *Phys. Lett. A* **160**, 571 (1991).
- [30] K. N. Joshipura and P. M. Patel, *Z. Phys. D* **29**, 269 (1994).
- [31] F. Salvat, J. D. Martinez, R. Mayol, and J. Parellada, *Phys. Rev. A* **36**, 467 (1987).
- [32] N. T. Padial and D. W. Norcross, *Phys. Rev. A* **29**, 1742 (1984).
- [33] J. P. Perdew and A. Zunger, *Phys. Rev. B* **23**, 5048 (1981).
- [34] X. Zhang, J. Sun, and Y. Liu, *J. Phys. B* **25**, 1893 (1992).
- [35] *Photon and Electron Interactions with Atoms, Molecules and Ions*, edited by Y. Itikawa, Vol. I 17C of Landolt-Börnstein: Numerical Data and Functional Relationships in Science and Technology – New Series (Springer, Berlin, 2003), and references therein.
- [36] M. Allan and L. Andric, *J. Chem. Phys.* **105**, 3559 (1996).
- [37] M. T. do N. Varella, L. G. Ferreira, and M. A. P. Lima, *J. Phys. B* **32**, 2031 (1999).
- [38] Cz. Szymkowski, Ł. Kłosowski, A. Domaracka, M. Piotrowicz, and E. Ptasińska-Denga, *J. Phys. B* **37**, 1833 (2004).
- [39] Cz. Szymkowski, M. Piotrowicz, A. Domaracka, Ł. Kłosowski, E. Ptasińska-Denga, and G. Kasperski, *J. Chem. Phys.* **121**, 1790 (2004).
- [40] Cz. Szymkowski and E. Ptasińska-Denga, *Vacuum* **63**, 545 (2001).
- [41] Cz. Szymkowski, A. Domaracka, P. Możejko, E. Ptasińska-Denga, Ł. Kłosowski, M. Piotrowicz, and G. Kasperski, *Phys. Rev. A* **70**, 032707 (2004).
- [42] *CRC Handbook of Chemistry and Physics*, 86th ed., edited by D. R. Lide, CDROM version (Taylor and Francis, Boca Raton, 2006); D. R. Lide and D. E. Mann, *J. Chem. Phys.* **29**, 914 (1958).
- [43] J. W. Au, G. Cooper, and C. E. Brion, *Chem. Phys.* **215**, 397 (1997).
- [44] K. J. Miller, *J. Am. Chem. Soc.* **112**, 8533 (1990).
- [45] Cz. Szymkowski, *Z. Phys. D* **13**, 69 (1989).